Hindawi
Wireless Communications and Mobile Computing
Volume 2022, Article ID 5877263, 10 pages
https://doi.org/10.1155/2022/5877263

Research Article

Millimeter Wave All-Around Antenna Based on Whispering Gallery Mode Dielectric Resonator for IoT-Based Applications

Alexander Kogut,[1] **Giuseppe Annino**,[2] **Mohamed El Bakkali**,[3] **Rachid Ahl Laamara**,[3] **Sandeep Kumar Arora**,[4] **D. S. Bhupal Naik**,[5] **and Fidele Maniraguha**[6]

[1]*O.Ya.Usikov Institute for Radiophysics and Electronics of NAS of Ukraine, Kharkiv, 12, Ac. Proskura St., 61085, Ukraine*
[2]*Istituto per I Processi Chimico-Fisici, IPCF-CNR, via G. Moruzzi 1, 56124 Pisa, Italy*
[3]*Faculty of Sciences of Rabat, Mohamed 5 University, Rabat, Morocco*
[4]*Lovely Professional University, Phagwara, Punjab, India*
[5]*Vignan's Foundation for Science, Technology and Research, India*
[6]*University of Rwanda, College of Science and Technology, Rwanda*

Correspondence should be addressed to Alexander Kogut; hazar70@gmail.com, Sandeep Kumar Arora; sandeep.16930@lpu.co.in, and Fidele Maniraguha; manifils@gmail.com

Received 1 April 2022; Revised 31 May 2022; Accepted 7 June 2022; Published 29 June 2022

Academic Editor: Kuruva Lakshmanna

This work is devoted to the study of the emitting properties of azimuthally inhomogeneous segmental dielectric resonators excited by whispering gallery modes. Due to the diffraction of the azimuthal waves on local nonhomogeneities located equidistantly along the azimuthal coordinate, intense electromagnetic radiation is achieved in the azimuthal sector of the angles 0°-360°. A prototype of an all-around emitting antenna based on basis of a segmental dielectric resonator is proposed, and its characteristics in the far zone are studied. It is shown that such an antenna forms a multilobe radiation pattern (72 lobes) in the circle sector of angles. The antenna gain in the lobes at the resonant frequency reaches 12 dB. Antenna optimization is achieved in the proposed method because of the large gain produced by the antenna. It is also analyzed that these types of radiation patterns observed by antennas are well used for the Internet of Things- (IoT-) based applications.

1. Introduction

The problem of frequency selection plays an important role in the fundamental and applied electromagnetism, partly due to the fact that the useful part of the electromagnetic spectrum spans a frequency interval of many decades, enabling many different areas of technology. In recent years, much attention has been paid to all those techniques related to the information processing, such as telecommunication systems, 5G-networks, radars, and data transmission systems [1–6].

In the field of communication, the current trend is to push the employed electromagnetic spectrum towards to the millimeter- (mm-) wave band. Such trend generates different challenges to researchers, due to the historical lack of components in this part of the electromagnetic spectrum. With the development of solid-state sources emitting at higher frequencies, the focus of research activities moved towards the passive components of mm-wave circuits. Among these components, a crucial importance can be attributed to electromagnetic resonators.

Resonators owe their importance to two peculiar (and interrelated) characteristics: first, their ability to select among different frequencies, due to a strongly frequency-dependent spectrum, and second, the possibility to store large amounts of electromagnetic energy. Resonators can be used to stabilize

the emission of a source [7], as well as to filter the electromagnetic signal propagating along a circuit [8]. In spectroscopic applications, the resonators are often employed as an effective sensing element, capable to improve the signal-to-noise of the measurement by orders of magnitude [9–11].

At microwaves, the most common resonators are given by closed metallic cavities acting as single-mode resonators [12], characterized by a resonance frequency occurring at a wavelength of the order of the dimension of the cavity.

Although very efficient, these resonators become increasingly difficult to use at high frequencies, due to their relatively small size and closed structure. The main drawbacks of the closed metallic cavities can be overcome employing open metallic cavities [13, 14] and open cavities based on metallic and dielectric elements [15], both operating as single-mode resonators.

At very high frequencies, however, working with single-mode resonators can become prohibitively difficult, owing to the extreme miniaturization that would be required. In this case, overmoded resonators appear as the most indicated choice, as in the case of the popular Fabry-Perot resonator [16]. In recent decades, another class of overmoded resonators, the dielectric resonators (DRs) operating on the so-called whispering gallery modes (WGMs), gained more and more popularity, thanks to their unique characteristics as simple monolithic structure, easy to build and integrate in electromagnetic circuits, and excellent spectral properties.

Historically, the dielectric resonators based on WGMs were first proposed in 1939 by Richtmyer [17]. For a relatively long period, their use was very limited. Starting from the eighties, the importance of the WGM resonators for mm-wave, subMM-wave, and visible-wave applications became more and more recognized [10, 11, 18–22]. Despite their simplicity, WGM resonators can combine extremely high quality factors with a well-resolved resonance spectrum [23], which makes these resonators an ideal candidate for many applications as electronic [20, 24–29], spectroscopy, and sensing [30, 31].

From the physical point-of-view, high-order modes, such as WGMs, are formed in the DRs as the result of the electromagnetic energy confinement due to the total internal reflection of the waves. The waves, propagating inside a dielectric structure in the form of a disk (ring) or a sphere, drop on its curved surface at small angles, lower than the critical angle, corresponding to a reflection coefficient at the dielectric-free space interface close to 1.0. Such a confinement mechanism proved very efficient, leading to a surprisingly weak dissipation of the electromagnetic energy stored in the resonator, corresponding to exceptional quality factors in case of very low dielectric loss materials [23].

The electromagnetic fields of WGMs are mainly localized inside the dielectric material of the resonator, in a "belt" region comprised between the internal caustic and the external caustic, the latter corresponding to the curved surface of the resonator. Outside the dielectric structure, the field intensity of the WGMs rapidly decreases already at distances comparable to the operating wavelength. The specific field distribution along the azimuthal coordinate (increasing along the curvilinear surface of the resonator) is a distinguishing feature of such oscillation modes. The typical distribution of the electric field of a standing-wave WGM observed in a dielectric disk is shown in Figure 1.

It can be seen that the regions with the highest intensity of the resonant electric field (bright areas in Figure 1) are regularly distributed along the azimuthal coordinate. The number of peaks of the electric field along the azimuthal coordinate defines the most important modal index of the WGM, usually indicated with the letter n [19]. The index n corresponds to the number of wavelengths of the radiation along the azimuthal coordinate. Accordingly, the number of electric field antinodes is $2n$.

Such an original distribution of the WGM's fields in DR, combined with the open structure of these resonators, makes it possible to create multifunctional devices for various purposes. In particular, locating several perturbing elements around the border of the DR, it is possible to alter in a controlled way both the electromagnetic spectrum and the emission properties.

2. Research Goals and Objectives

In this paper, it is proposed to consider a new promising field of application of DRs operating with WGMs. In particular, the possibility to alter in a controlled way the emission properties of the WGM DRs gives the opportunity to develop a simple and innovative concept of antennas, characterized by a circular emission pattern. In these systems, the modification of the border of the DR needs to be compatible with the general structure of the standing-wave WGM resonant fields, in order to preserve the nature of the resonance mode. Nevertheless, the modification needs to be profound enough to provide an efficient radiation of energy, still keeping a resonant behavior, which is essential for a good coupling of the incoming radiation to the device. Such constraints can be respected by introducing a regular distribution of local nonuniformities into the design of the disk DR, which is synchronized with the electric field pattern of the WGM mode. As a result, it is expected that the radiation of an antenna based on such a nonuniform disk DR will be formed by diffraction of the waves generated by each local nonuniformities introduced in the border of the disk. In this case, the regular distribution of the scattering centers along the boundary of the disk, placed in correspondence of the antinodes of the electric field, provides a high-intensity radiation in the far zone. This radiation reproduces the circular distribution of the scattering elements.

Similar resonant type dielectric structures were previously considered in relation with the optical wavelength range. In research works presented by [32–35], the designs and operational features of the so-called "microgear resonators" were discussed and considered as basic elements of lasers in the optical range [36–40]. In [41], the optimization of the conditions for the excitation of WGMs in such resonators by electromagnetic coupling with a waveguide is proposed. All previous studies of DR in the shape of gears were related to the optical range. In this study, the possibility of using the properties of DRs with local azimuthal nonuniformities as a controllable radiating element at Ka-band (millimeter waves) is proposed. The importance of the proposed

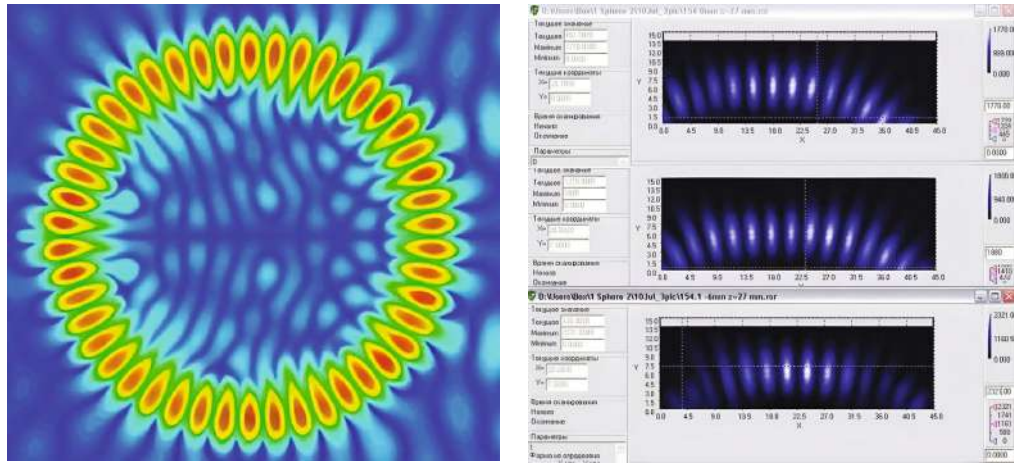

Figure 1: E-field distribution of a standing-wave WGM of a dielectric disk made with a low dielectric loss material (simulation and experiment).

study is twofold. First, to demonstrate that the concept of a spectral emission controlled by means of a modification of the border of an overmoded dielectric resonator is effective also at mm-wave frequencies, where strategic communication technologies are currently under development. Second, to show that such an approach can be implemented in a very simple configuration.

Because digitization of a huge volume of data is being generated across the several sectors such as health care, manufacturing and production, and Internet of Things (IoT), IoT in healthcare system will give the significant analysis using the big data-based analysis. Machine learning algorithms are used to predict the data pattern for targeting decisions in a right direction [42, 43]. In addition to that, many learning mechanisms are used for predicting the data. Deep neural network is one of them and used for predicting the battery life in integration with IoT [44]. Three-step DNA sequence mining is also proposed for optimization of the search results using the machine learning approach [45–48].

The perturbing element proposed in this paper is given by small air gaps, radially oriented with respect to the axis of the resonator and placed in correspondence of the antinodes of the WGM electric field, as illustrated in Figure 2(a). The width of the air gaps should be selected in such a way that the electric field antinodes with opposite phase (0 and π) should be located on the edge of each segment (bright red and blue spots in Figure 2(b)), in order to maximize the scattering and thus the emission efficiency. The number of field antinodes is twice with respect to the azimuthal modal index n of the WGM, as anticipated, whereas the number of air gaps is equal to n. The electromagnetic fields characterizing the WGM modes of the segmental DR can be calculated in approximate way by using the analytical expressions reported in [19]; a rigorous analysis can be done by using advanced simulation software, such as CST Microwave Studio or COMSOL Multiphysics [49, 50].

The precise correspondence between the modal index n and the number of the equidistant gaps in the border of the resonant disk, illustrated by the field distribution of Figure 2(b), suggests that a coherent overlap of the fields radiated by the gaps can be obtained in the far field along specific directions, as desirable for an efficient antenna with circular emission pattern. The experimental verification of this concept at a resonant wavelength of $\lambda_0 \approx 8$ mm is the main goal of this work.

3. Research Objective and Methods

In this research work, we consider a disk made of Teflon with radius of 40 mm and height of 7.2 mm, with a segmental border shaped as shown in Figure 2(a), with a number of segment given by $N = 36$. As anticipated, the most natural WGM to consider for our purposes is the one with azimuthal index $n = 36$, which enables a period correspondence between the electric field and the profile of the segmental DR and determines the multiplicity of the circular scanning sector 00-3600 to the number of segments ($N = 36$). The shape of each segment must be such that the border of the segment corresponds to an antinode of the selected standing wave WGM, as shown in Figure 2(b). The exact shape of the segments has been determined with the help of numerical simulations based on CST Microwave Studio. The resulting segments have a shape close to trapezia with the maximal width on the edge of the segmental DR. The maximal width of each segment is ds ≈ 5.5 mm, determined taking into account the real part of the dielectric permittivity of Teflon at the frequencies of interest, $\varepsilon' = 2.08$. Following the same concept, the height of each air gap is chosen dg ≈ 1.5 mm. In the calculation of these dimensions, it was necessary to take into account that the wavelength of the radiation in the resonator is not simply related to the wavelength in vacuum and to the dielectric permittivity of the material forming the resonator. This is due to the fraction of electromagnetic energy distributed outside the disk and between the segments. Accordingly, a rigorous determination of the optimal dimensions of the air gaps requires the aid of numerical methods.

As mentioned above, the fields of WGMs in the DR are limited along the radial coordinate by the internal caustic. Its calculation is detailed in [19]. The radial depth of the air gaps in the segmental DR design should be close to the location of the WGM internal caustic. In this work, the radial depth of each air gap is equal 8 mm.

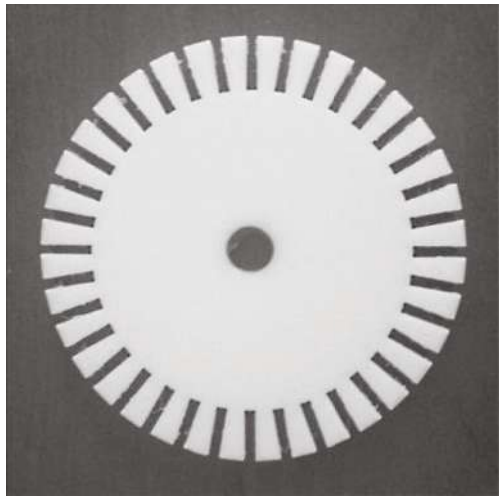

Fabricated DRA

(a) Fabricated DRA

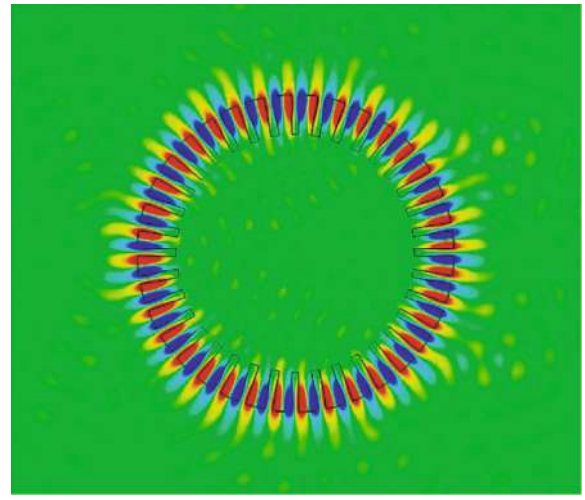

Distribution of the amplitude of WGM E-field

(b) Distribution of the amplitude of WGM E-field

Figure 2: Segmental DRA and its distribution of the amplitude of WGM E-field.

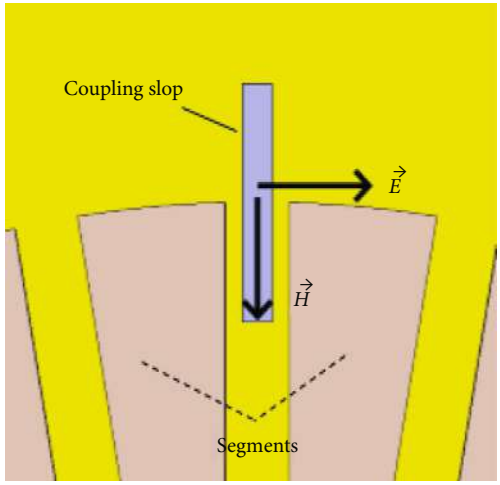

Figure 3: An arrangement of the coupling slot in a design of the segmental DR for excitation of operating WGMs.

The choice of the element for coupling the electromagnetic energy of an external source to the antenna is crucial in the achievement of an efficient radiant system. A coupling element in the form of a narrow coupling slot proved to be an efficient solution for the excitation of the proposed device, as discussed in [24, 37]. The excitation configuration is obtained placing the segmental dielectric structure on a flat conducting mirror (copper) that includes the coupling slot. A rectangular coupling slot with dimensions of 7.2×0.5 mm formed starting by the narrowed open end of a WR28 rectangular waveguide, 7.2×3.4 mm. The larger side of the coupling slot is oriented parallel to faces of segments, as shown in Figure 3. This provides the excitation of quasi TE-WGMs in the segmental DR, which are characterized by an electric field almost parallel to that emerging from the coupling slot.

Moreover, the electric field generated by the coupling slot does not propagates along the azimuthal direction of the segmental disk. This field is thus effective in exciting standing wave modes in the segmental DR.

The excitation efficiency and the field distribution in the coupling region and in the resonator were investigated with the support of computer simulation based on CST Microwave Studio 2016. These results were complemented by an experimental study on the radiation characteristics of the segmental DR antenna. The setup employed to characterize the emission pattern of the proposed device is schematically shown in Figure 4. The excitation of the segmental DR (element 1) is based on a narrow-band tunable oscillator (element 2), emitting in the frequency range 36.0-40.0 GHz and a waveguide (element 3).

The signal emitted by the antenna was received by a horn antenna (element 4) with an aperture of $50 \times 40\,\text{mm}^2$. The receiving horn was located in the far zone of the antenna at a distance of 1.5 m from it. It scans the field in the far zone of the antenna in a plane perpendicular to the direction of the Poynting vector.

The Poynting vector is directed parallel to the radius of the segmental DR and perpendicular to its flat bases. The horn was automatically movable along the azimuthal coordinate within sector of the angles 0°-360° by means of a step motor (element 5). The signal produced by the horn antenna was directed to a selective amplifier (element 7) through a coaxial line (element 6). The obtained signal was registered on a digital voltmeter (element 8), which made it possible to estimate the time average of the E-field intensity in the antenna far zone. The measurements were carried out at displacement of the horn antenna in the azimuth direction with a step of 1°.

4. Results and Discussions

In the study of the emission characteristics of the proposed antenna, the first point to investigate is its frequency response, given by a combination of the spectrum of the original DR and the effects of the modification of its border. Being the latter

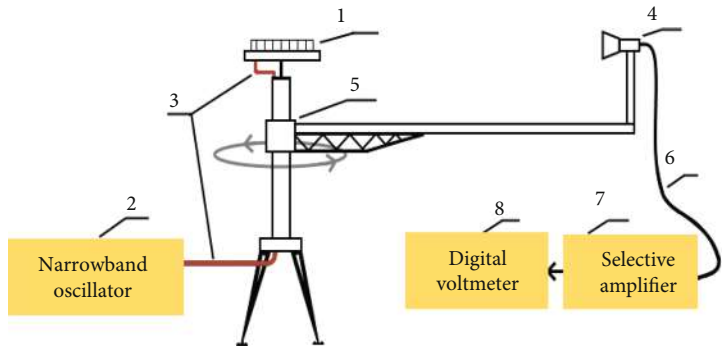

Figure 4: The schematic representation of the research facility.

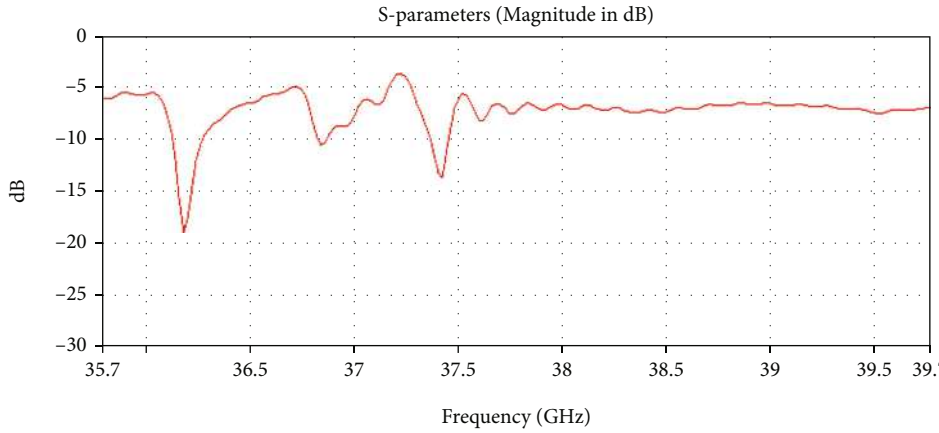

Figure 5: *S*-parameter of the antenna based on the segmental DR.

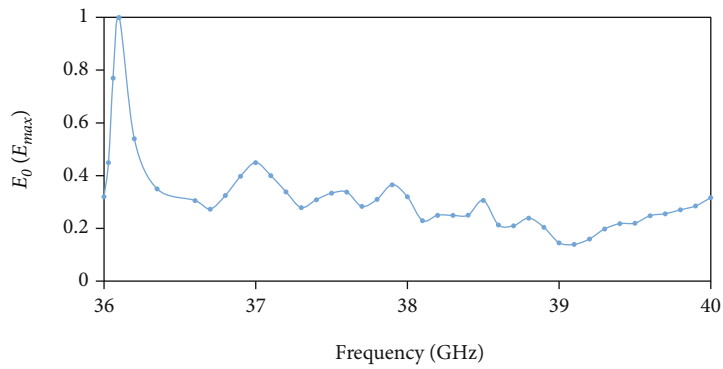

Figure 6: The dependence of the relative E-field intensity in the far zone of the antenna on the frequency of the reference signal.

periodical, a further selection is operated in terms of the allowed resonance frequency. Choosing the period of the border modifications that corresponds to the period of a given WGM, the resulting spectrum of the segmental DR will be very simplified, with a response peaked around the selected WGM. This effect is demonstrated in Figure 5, reporting the calculated *S*-parameter of the segmental DR in the frequency range 35.70-39.70 GHz.

The difference in frequency values between experiment and calculation does not exceed 0.2%. The calculated *Q*-factor of the segmental DR at resonant frequency $f \approx 36$ GHz is of the order of 300; corresponding -3 dB bandwidth is about 120 MHz, still high enough to provide an efficient coupling to the resonator and a clear spectrum of well-separated resonances. The electric field of this mode is reported in Figure 2(b).

Above this frequency, two other modes are visible, around 36.8 and 37.4 GHz, although broader and less coupled. For these modes, the correspondence between the position of the electric field antinodes and the position of the segments in the border of the disks is less accurate. As a result, a destructive interference among the standing waves generated by the segments starts to occur, which weakens and eventually cancels the resonance effect within the segmental DR, at higher frequencies. Above 38 GHz, no resonances are visible.

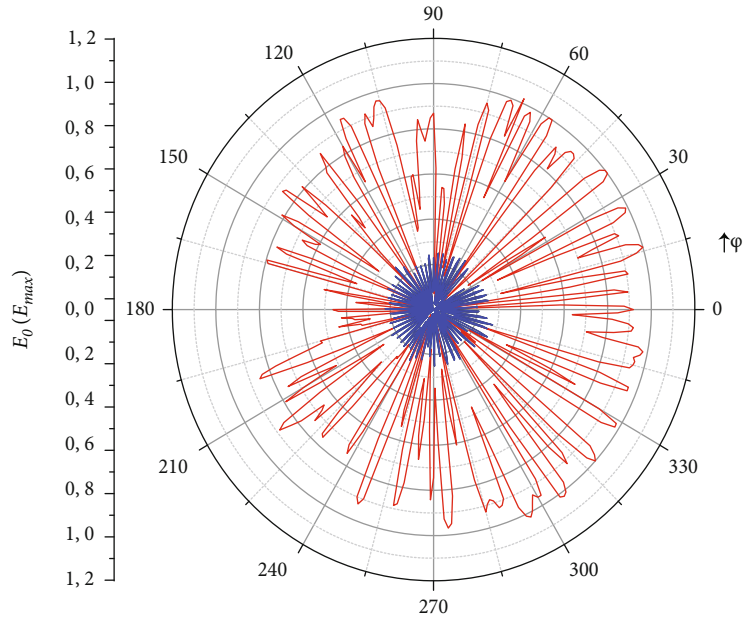

Figure 7: Radiation patterns of the antenna based on the segmental DR and homogenous dielectric disk at resonance frequencies of WGMs around 36 GHz.

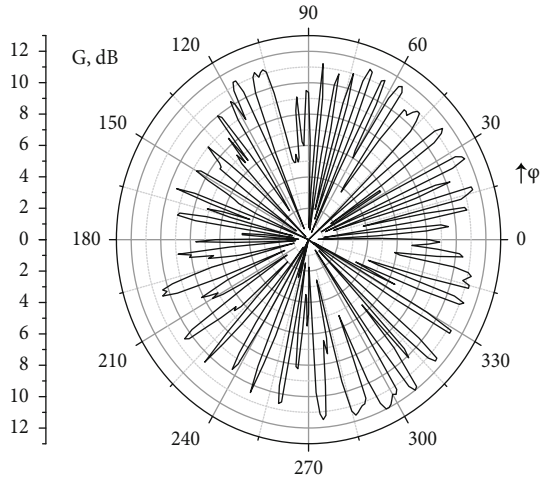

Figure 8: The dependence of the gain G of the antenna with two supplying slots on the azimuthal coordinate φ at the operating frequency $f = 36.08$ GHz.

The calculated behavior of the segmental DR is confirmed by the experimental study conducted on the segmental DR with the setup shown in Figure 4. In particular, Figure 6 shows the dependence of the relative E-field intensity $E_0/E_{\max}$ (E_0 is the current value of intensity, and $E_{\max}$ is the maximal value) in the far zone of the antenna on the frequency range of 36-40 GHz, for a fixed position of the detecting horn.

From Figure 6, it can be seen that the highest E-field intensity in the far zone of the antenna is achieved at a frequency of $f = 36.08$ GHz. The results of computer simulation show that this frequency is close to the calculated resonance frequency of the segmental DR. At this frequency, the antinodes of the electric field of the excited WGM with azimuthal index $n = 36$ are located at the edges of each of the segments (Figure 2(b)). At frequencies higher than that of the mode $WGM_{36,0,0}$, the spectrum of the resonator is rapidly flattened by the segmentation in the border of the disk, which interferes destructively with the standing wave of the other resonance modes, as shown by Figure 6(b) for the resonance frequency 36.8 and 37.4 GHz.

Figure 7 shows the antenna radiation pattern at the resonance frequency of $f = 36.08$ GHz, reported as the dependence of the relative E-field intensity $E_0/E_{\max}$ on the azimuthal coordinate φ of the receiving horn (red curve). The resulting radiation pattern has a multilobe structure and covers the entire azimuthal sector of the angles 0°-360°. Moreover, in some azimuthal sectors, adjacent lobes are added up. The numerical simulations show that the air gaps are the radiating elements of the antenna, each gaps providing two emission lobes, corresponding to the number of antinodes of the electric field per gap. Thus, an antenna based on a segmental DR with 36 segments forms a 72-lobe radiation pattern, resulting from the constructive interference of the waves emitted from the edges of adjacent segments. The width of each lobe at the -3.0 dB level is about 3.5°.

The secondary extra lobes detected in the far field emission of the disk are probably due to the small imperfections in the cutting of the air gaps.

For comparison, Figure 7 also shows the radiation pattern of a uniform Teflon disk having the same diameter and thickness of the segmental one. The resonance frequency is about 36.22 GHz and is close to the resonance frequency of the considered segmental DR (blue curve). It can be seen that the intensity of the E-field in the far zone of the antenna based on the unperturbed DR disk is much lower than that based on the segmental DR. The highest intensity of the E-field in the far zone of the unperturbed DR disk is more than 4 times less than the E-field intensity of the segmental DR. This is

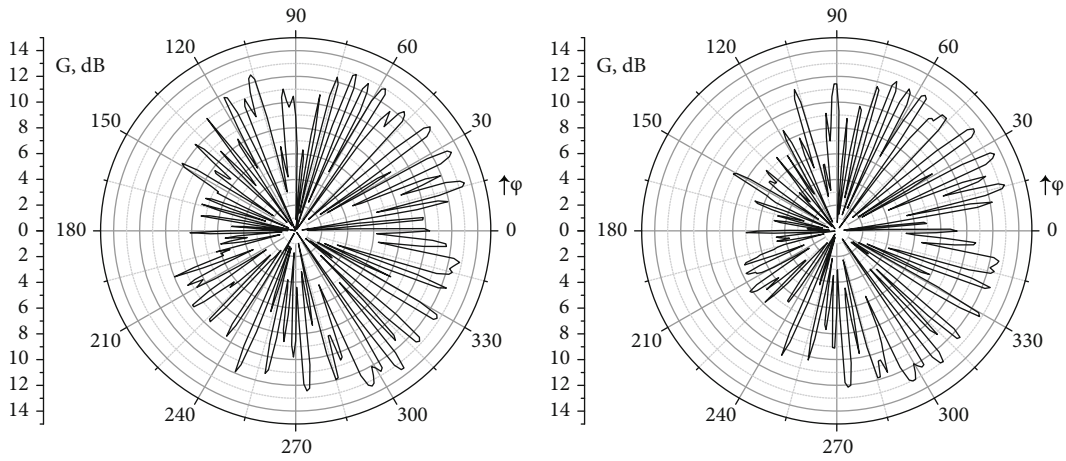

(a) $f = 36.05$ GHz (b) $f = 36.11$ GHz

Figure 9: The dependence of a gain of the antenna based on the segmental DR on an azimuthal coordinate φ at frequencies 36.05 GHz (a) and 36.11 GHz (b).

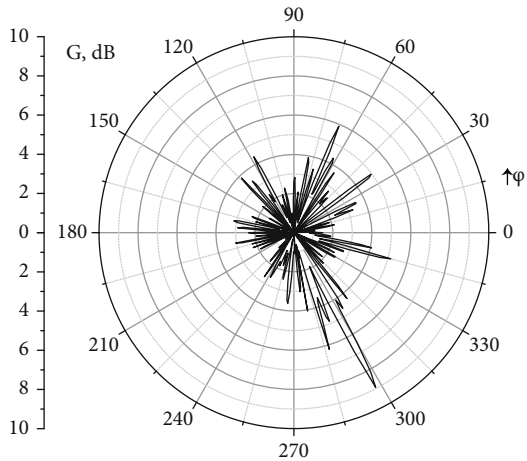

Figure 10: The dependence of a gain of the antenna based on the segmental DR on an azimuthal coordinate φ at a frequency of 36.40 GHz.

explained by the low radiation emission of the WGMs of a uniform disk DR. In this case, most of the energy of the electromagnetic field is stored in the resonator and dissipated by heat at their resonance frequencies. For this reason, a homogeneous DR disk DR has a significantly higher Q-factor as compared to a segmented DR. The unloaded Q-factor of the uniform disk DR is $Q \approx 4200$. The relevant reduction of the quality factor of the segmental DR is due to the strong increase of its radiation losses, necessary for the device to act as an efficient antenna.

It is worthwhile to note that a "shadow" area in the antenna radiation pattern of the segmental DR is formed in the sector of angles 165°-195° (Figure 7). The coupling slot feeding the antenna is placed in this angle sector, being its center placed at the azimuthal coordinate of 180°. The coupling slot represents itself a local perturbing element for the WGM fields, corresponding to a perturbation in the emission pattern. To eliminate this negative effect, it is proposed to use two supplying elements, identical in size, located symmetrically with respect to the segmental dielectric structure. For this purpose, a second coupling slot with similar dimensions is located in the metal mirror of the segmental DR, at azimuthal coordinate of 0°. The energy of the electromagnetic field is supplied to both coupling slots from a common narrowband oscillator, now equipped with a directional coupler is used in the supplying waveguide line.

Figure 8 shows the dependence of the gain G of the antenna with the two supplying elements on the azimuthal coordinate φ, at the operating frequency $f = 36.08$ GHz.

It can be seen that using two symmetrically located coupling elements makes it possible to achieve a close to uniform distribution of lobes in the entire sector of azimuthal angles 0°-360°. As in the case of using one supplying element, the number of lobes in the antenna radiation pattern is 72 units. The width of each lobe at the level of -3.0 dB is close to 3.5°.

The high values of the gain in the lobes at the resonant frequency of the segmental DR are one of the main advantages of the proposed antenna. Figure 7 shows that the antenna gain can reach 12 dB. Such high values of the antenna gain are determined by the high E-field intensity in the area of radiation—the emitting edges of the segments. The analysis of the emission pattern in the axial direction shows that the width of the radiation pattern of the proposed antenna in elevation is about 10°.

Figures 9(a) and 9(b) show the dependence of the antenna gain G on the azimuthal coordinate φ detuning the excitation frequency by 30 MHz to the low- and high-frequency regions relatively the central resonance value of 36.08 GHz.

It can be seen that with a relatively small detuning of the excitation frequency of the resonant antenna, a large "shadow" region is formed in its emission pattern. It is associated to a violation of the resonance condition at the basis of the field structure of the WGM.

Figure 10 shows the dependence of the antenna gain G on the azimuthal coordinate φ at a large detuning of the excitation frequency, given now by 320 MHz above the resonance frequency of 36.08 GHz.

It can be seen that at a frequency well outside the resonant response, the proposed antenna does not form a significant radiation pattern in the entire azimuthal sector of angles 0°-360°. This is determined by the absence of intense electric fields in the segmental DR. The appearance of individual lobes is associated with random reflection of waves from individual segments.

5. Conclusion

In this work, it is shown that dielectric resonant structures operating with whispering gallery modes can be used to create efficient all-around antennas by introducing periodic local nonuniformities on their curved surfaces. The proposed devices combine the benefits of the resonant systems, characterized by a selective frequency response and by an efficient excitation, in which all the electromagnetic power delivered by the source can be transferred to the device, together with those of large emission pattern antennas. In the investigated system, the antenna forms a multilobe (72 units) radiation pattern in the azimuthal sector of angles 0°-360° at the central resonance frequency, with the lobes having a width of about 3.50 at -3.0 dB level. In the radiation lobes, the gain of the antenna is as high as $G = 12$ dB. The radiating properties of the antenna are retained in the frequency range delimited by the resonant response. In the investigated case, it corresponds to frequency interval of about 120 MHz, centered around the resonance frequency of 36 GHz.

The device investigated in this work is based on a dielectric disk made of Teflon, having a diameter of 40 mm and a thickness of 7.2 mm. Much more compact segmental DR antennas can be obtained employing low dielectric loss and high index of refraction materials.

The obtained results can represent an important contribution in the development of advanced communication technologies at millimeter and submillimeter wavelengths.

Data Availability

The data is available on request.

Conflicts of Interest

The authors declare that they have no conflicts of interest.

Acknowledgments

The authors would like to thank Prof. Dr. Igor Kuzmichev, Prof. Dr. Roman Dolia, Prof. Dr. Sergey Nosatiuk (O.Ya. Usikov Institute for Radiophysics and Electronics of NAS of Ukraine, Kharkiv, Ukraine), and Prof. Dr. Niamat Hussain (Sejong University, Seoul, Republic of Korea) for sharing their knowledge on subMM-wave spectrum and their extreme support in preparing this research work. This work is funded by the University of Rwanda, African Center of Excellence in Internet of Things, Kigali.

References

[1] S.-Q. Xiao and M.-T. Zhou, *Millimeter Wave Technology in Wireless PAN, LAN, and MAN*, Auerbach Publications Taylor & Francis Group, 2008.

[2] S. M. Hashima, "Digital communication systems, Ministry of Higher Education Tanta Higher Institute Of Engineering & Technology Communication & Computer Engineering Dept," 2018, [Online], Available: https://www.researchgate.net/publication/329170465_Digital_Communication_Systems.

[3] M. El-Saba, *Fundamentals of Communication Systems & Networks*, Hakim Press, Cairo, 2015.

[4] M. Z. Noohani and K. U. Magsi, "A review of 5G technology: architecture, security and wide applications," *International Research Journal of Engineering and Technology (IRJET)*, vol. 7, no. 5, p. 34, 2020.

[5] S. Hosain, "5G wireless communication systems," *American Journal of Enhineering Reasearch*, vol. 2, no. 10, pp. 344–353, 2013.

[6] S. Honma and N. Uehara, "Millimeter-wave radar technology for automotive application, technical reports," 2001, [Online], Available: http://www.mitsubishielectric.com/bu/automotive/advanced_technology/pdf/vol94_tr5.pdf.

[7] G. J. Dick and J. Saunders, "Measurement and analysis of a microwave oscillator stabilized by a sapphire dielectric ring resonator for ultra-low noise," *IEEE Transactions on Ultrasonics, Ferroelectrics, and Frequency Control*, vol. 37, no. 5, pp. 339–346, 1990.

[8] J. Lee, S. Pinel, J. Laskar, and M. M. Tentzeris, "Design and development of advanced cavity-based dual-mode filters using low-temperature co-fired ceramic technology for V-band gigabit wireless systems," *IEEE Transactions on Microwave Theory and Techniques*, vol. 55, no. 9, pp. 1869–1879, 2007.

[9] C. P. Poole, *Electron Spin Resonance: A Comprehensive Treatise on Experimental Techniques*, Wiley, New York, 1983.

[10] C. Vedrenne and J. Arnaud, "Whispering-gallery modes of dielectric resonators," *IEE Proceedings H (Microwaves, Optics and Antennas)*, vol. 129, no. 4, pp. 183–187, 1982.

[11] "Chapter 3., Dielectric resonator and whispering gallery mode resonator," [Online], Available: https://pdfs.semanticscholar.org/9053/46a7ca2c7170c17ec06e0f57cd1f90b33177.pdf.

[12] W. W. Hansen, "A type of electrical resonator," *Journal of Applied Physics*, vol. 9, no. 10, pp. 654–663, 1938.

[13] G. Annino, M. Cassettari, and M. Martinelli, "Open nonradiative cavities as millimeter wave single-mode resonators," *Review of Scientific Instruments*, vol. 76, no. 6, article 064702, 2005.

[14] G. Annino, M. Cassettari, and M. Martinelli, "A new concept of open TE_{011} cavity," *IEEE Transactions on Microwave Theory and Techniques*, vol. 57, no. 4, pp. 775–783, 2009.

[15] G. Annino, M. Cassettari, and M. Martinelli, "Axially open nonradiative structures: an example of single-mode resonator based on the sample holder," *Review of Scientific Instruments*, vol. 76, no. 8, article 084702, 2005.

[16] W. Culshaw, "Resonators for millimeter and submillimeter wavelengths," *IRE Transactions on Microwave Theory and Techniques*, vol. 9, no. 2, pp. 135–144, 1961.

[17] R. D. Richtmyer, "Dielectric resonators," *Journal of Applied Physics*, vol. 10, no. 6, pp. 391–398, 1939.

[18] G. Annino, M. Cassettar, I. Longo, and M. Martinelli, "Whispering gallery modes in a dielectric resonator: characterization at millimeter wavelength," *IEEE Transactions on Microwave Theory and Techniques*, vol. 45, no. 11, pp. 2025–2034, 1997.

[19] G. Annino, M. Cassettari, and M. Martinelli, "Study on planar whispering gallery dielectric resonators. I. General properties," *International Journal of Infrared and Millimeter Waves*, vol. 23, no. 4, pp. 597–615, 2002.

[20] G. Annino, M. Cassettari, and M. Martinelli, "Study on planar whispering gallery dielectric resonators. II. A multiple-band device," *International Journal of Infrared and Millimeter Waves*, vol. 23, no. 4, pp. 617–634, 2002.

[21] J. R. Wait, "Electromagnetic whispering gallery modes in a dielectric rod," *Radio Science*, vol. 2, no. 9, pp. 1005–1017, 1967.

[22] D. Kajfez and P. Guillon, *Dielectric Resonators*, vol. 4, Artech House, Norwood, MA, 1986.

[23] V. B. Braginsky, V. S. Ilchenko, and K. S. Bagdassarov, "Experimental observation of fundamental microwave absorption in high-quality dielectric crystals," *Physics Letter A*, vol. 120, no. 6, pp. 300–305, 1987.

[24] A. E. Kogut, Z. E. Eremenko, I. K. Kuzmichev, R. S. Dolia, and M. T. Islam, "Power summation of the Gunn-diodes in the ultra-thin planar dielectric resonator," in *2019 49th European Microwave Conference (EuMC)*, Paris, France, 2019.

[25] A. E. Kogut, I. K. Kuz'michev, R. S. Dolia, S. O. Nosatiuk, and Y. A. Shulga, "Possibility for frequency stabilization of millimeter wavelength solid-state source by a screened dielectric resonator," *Astronomy*, vol. 21, no. 4, pp. 311–317, 2016.

[26] Z. Eremenko, A. Shubny, A. Kogut, and R. Dolia, "Comparison of high loss liquids dielectric properties measurement using waveguide and resonator methods," in *Proceedings of European Microwave Conference in Central Europe (EuMCE2019)*, pp. 519–523, Prague, Czech Republic, May 2019.

[27] Kogut, "Millimeter wave technique based on dielectric resonators/ new results and applications," in *EngiTek 2020 - Conferences*, Jordan, 16-18 June, 2020.

[28] A. K. Kirichenko, "Gunn-oscillator stabilized by the dielectric resonator for measuring the electrical characteristics of liquids," *Electromagnetic waves and electron systems*, vol. 12, no. 2, pp. 57–59, 2007, in Russian.

[29] A. Kirichenko and A. E. Kogut, "Dielectric half-disk resonator with whispering-gallery modes for measurements of the electric properties of water," *Radiophysics and Quantum Electronics*, vol. 51, no. 9, pp. 695–701, 2008.

[30] G. Annino, M. Cassettari, I. Longo, M. Martinelli, P. J. M. Van Bentum, and E. van der Horst, "A novel probe head for high-field, high-frequency electron paramagnetic resonance," *Review of Scientific Instruments*, vol. 70, no. 3, pp. 1787–1793, 1999.

[31] X. F. Jiang, A. J. Qavi, S. H. Huang, and L. Yang, "Whispering-gallery sensors," *Matter*, vol. 3, no. 2, pp. 371–392, 2020.

[32] M. Fujita and T. Baba, "Proposal and finite-difference time-domain simulation of whispering gallery mode microgear cavity," *IEEE Journal of Quantum Electronics*, vol. 37, no. 10, pp. 1253–1258, 2011.

[33] K. P. Huy, A. Morand, and P. Benech, "Modelization of the whispering gallery mode in microgear resonators using the Floquet-Bloch formalism," *IEEE Journal of Quantum Electronics*, vol. 41, no. 3, pp. 357–365, 2005.

[34] K. Nozaki, A. Nakagawa, D. Sano, and T. Baba, "Ultralow threshold and single-mode lasing in microgear lasers and its fusion with quasi-periodic photonic crystals," *IEEE Journal of Selected Topics in Quantum Electronics*, vol. 9, no. 5, pp. 1355–1360, 2003.

[35] M. Fujita and T. Baba, "Microgear laser," *Applied Physics Letters*, vol. 80, no. 12, pp. 2051–2053, 2002.

[36] E. M. Amhoud, E. Awwad, G. R. Ben-Othman, and Y. Jaouën, "Mode selection and larger set equalization for mode-multiplexed fiber transmission systems," in *2015 Optical Fiber Communications Conference and Exhibition (OFC)*, pp. 1–3, Los Angeles, CA, USA, 2015.

[37] E. M. Amhoud, M. Chafii, A. Nimr, and G. Fettweis, "OFDM with index modulation in orbital angular momentum multiplexed free space optical links," in *2021 IEEE 93rd Vehicular Technology Conference (VTC2021-Spring)*, pp. 1–5, Helsinki, Finland, 2021, April.

[38] E. M. Amhoud, G. R. B. Othman, and Y. Jaouën, "Concatenation of space-time coding and FEC for few-mode fiber systems," *IEEE Photonics Technology Letters*, vol. 29, no. 7, pp. 603–606, 2017.

[39] E. M. Amhoud, G. R. B. Othman, and Y. Jaouën, "Design criterion of space-time codes for SDM optical fiber systems," in *2016 23rd International Conference on Telecommunications (ICT)*, pp. 1–5, Thessaloniki, Greece, 2016, May.

[40] E. M. Amhoud, G. R. B. Othman, L. Bigot et al., "Experimental demonstration of space-time coding for MDL mitigation in few-mode fiber transmission systems," in *2017 European Conference on Optical Communication (ECOC)*, pp. 1–3, Gothenburg, Sweden, 2017, September.

[41] V. M. N. Passaro, F. D. Leonardis, and G. Z. Mashanovich, "Investigation of coupling conditions in microgear resonators," *Optics Express*, vol. 15, no. 3, pp. 797–808, 2007.

[42] K. Lakshmanna and N. Khare, "Constraint-based measures for DNA sequence mining using group search optimization algorithm," *International Journal of Intelligent Engineering & systems*, vol. 9, no. 3, pp. 91–100, 2016.

[43] A. Priyanka, M. Parimala, K. Sudheer, R. Kaluri, K. Lakshmanna, and M. P. Reddy, "BIG data based on healthcare analysis using IOT devices," *IOP Conference Series: Materials Science and Engineering*, vol. 263, no. 4, article 042059, 2017.

[44] R. Kaluri, D. S. Rajput, Q. Xin et al., "Roughsets-based approach for predicting battery life in IoT," 2021, https://arxiv.org/abs/2102.06026.

[45] K. Zerhouni, E. M. Amhoud, and M. Chafii, "Filtered multicarrier waveforms classification: a deep learning-based approach," *IEEE Access*, vol. 9, pp. 69426–69438, 2021.

[46] A. Azougaghe, Z. Kartit, M. Hedabou, M. Belkasmi, and M. El Marraki, "An efficient algorithm for data security in cloud storage," in *Intelligent Systems Design and Applications (ISDA)*, Marrakech, Morocco, 2015.

[47] M. Azougaghe, O. O. Hedabou, M. Belkasmi, and A. Kobbane, "Many-to -one matching game towards secure virtual machine migrating in cloud computing," in *International Conference on Advanced Communication System and Information Security*, Marrakesh, Morocco, 2016.

[48] G. S. Gaba, M. Hedabou, P. Kumar, A. Braeken, M. Liyanage, and M. Alazab, "Zero knowledge proofs based authenticated key agreement protocol for sustainable healthcare," *Sustainable Cities and Society*, vol. 80, p. 103766, 2022.

[49] "CST Studio Suite Simulator," [online Available]: https://www.3ds.com/products-services/simulia/products/cst-studio-suite/.

[50] COMSOL, "Multiphysics® software," [online Available]: https://www.comsol.com/.